Momentum distribution and final-state effects in liquid ^{4}He

K. H. Andersen
Institut Laue-Langevin, Boîte Postale 156, 38042 Grenoble Cedex 9, France

W. G. Stirling*
Department of Physics, Keele University, Keele, Staffordshire ST5 5BG, United Kingdom

H. R. Glyde
Department of Physics and Astronomy, University of Delaware, Newark, Delaware 19716-2570
(Received 27 May 1997)

Neutron time-of-flight measurements of the dynamic structure factor $S(Q,\omega)$ of both normal liquid and superfluid ^{4}He are presented. Using the MARI spectrometer at the ISIS pulsed neutron source (U.K.), $S(Q,\omega)$ was measured over continuous ranges in wave vector Q up to 10 Å^{-1} at a temperature of 1.42 K, while at $T=2.5$ K the range extended up to $Q=17$ Å^{-1}. The quality of the data represents a significant increase in statistical precision over previous measurements. The width and peak position of $S(Q,\omega)$ at both temperatures is seen to oscillate as a function of Q; this is due to coherence effects and has been observed in previous measurements. These oscillations are seen to continue up to a wave vector in excess of 10 Å^{-1}. For the $T=2.5$ K data, the measured $S(Q,\omega)$ spectra are analyzed using the technique developed by Glyde. Three free parameters are fitted at each Q and very good agreement is obtained. The Q scaling of these parameters is used to extract information about the shape of the normal fluid momentum distribution $n(\mathbf{p})$, which is found to be distinctly non-Gaussian and in good agreement with Monte Carlo calculations. The mean kinetic energy per atom is obtained from the data and is in good agreement with previous neutron and x-ray work. [S0163-1829(97)00238-5]

I. INTRODUCTION

The objective of neutron-scattering measurements at high momentum transfer is to determine the dynamics of single atoms in liquids and solids.[1,2] The observed dynamic structure factor $S(Q,\omega)$ depends on the atomic momentum distribution $n(\mathbf{p})$, the related atomic kinetic energy $\langle K\rangle$, and the interaction of the atoms with its neighbors. Physically, a high-energy incoming neutron interacts with and scatters from a single atomic nucleus. The entire struck atom recoils. At constant momentum transfer $\hbar Q$ to the atom, the energy transferred is ''Doppler broadened'' by the initial momentum distribution of the atom, rather than being constant at the stationary, free atom recoil energy $\hbar\omega_r=(\hbar Q)^2/2m$. This broadening is used to determine $n(\mathbf{p})$. However, the interaction of the recoiling struck atom with its neighbors modifies this broadening. A reliable description of this interaction, denoted the final-state (FS) effects, is needed to extract $n(\mathbf{p})$.[3–8]

At lower momentum transfer, the interaction of the struck atom with its neighbors has a major impact on $S(Q,\omega)$, coherent effects between the atoms are important and the goal is usually to investigate these interactions. As Q increases, coherent effects become negligible, $S(Q,\omega)$ reduces to the incoherent limit $S_i(Q,\omega)$, and $n(\mathbf{p})$ can be determined. However, a good determination of FS effects is always required. Only in the limit of the impulse approximation[1,2] (IA) in which

$$S_{\mathrm{IA}}(Q,\omega)=\int \delta\left(\omega-\omega_r-\frac{\mathbf{p}\cdot\mathbf{Q}}{m}\right)n(\mathbf{p})\,d\mathbf{p} \qquad (1)$$

does the observed dynamic structure factor $S(Q,\omega)$ depend solely on $n(\mathbf{p})$. The Q values required to reach this limit in real materials is not clear.

In quantum liquids, the initial goal[9,10] of high Q measurements was to determine the condensate fraction $n(\mathbf{p}=0)=n_0$ in superfluid ^{4}He. Early measurements, which led to a wide spectrum of n_0 values, are reviewed by Martel *et al.*[11] Sears *et al.*[12,13] obtained reliable values of $n_0=13.9\pm2.3\%$ and $n_0=10.9\pm2.7\%$ using two sets of data taken at $Q\approx10$ Å^{-1}. The new feature was a reliable description of FS contributions.[14] From measurements at significantly higher Q values ($Q\approx30$ Å^{-1}) using spallation source neutrons, Sokol and co-workers[15–18] obtained $n_0=10\pm2\%$, the temperature dependence of $n_0(T)$, and many other properties of superfluid and normal ^{4}He. These measurements used the FS broadening function calculated by Silver.[5] The field is extensively reviewed by Glyde and Svensson,[19] Sokol,[20] and Glyde.[21]

In the lower wave vector range $4<Q<10$ Å^{-1}, Cowley and Woods,[22] Martel *et al.*,[11] and Stirling *et al.*[23] showed that the peak position and half-width of the observed $S(Q,\omega)$ in liquid ^{4}He oscillated with Q. These oscillations arise from coherence effects since in the incoherent limit ($Q>12$ Å^{-1}), $S_i(Q,\omega)$ cannot oscillate. These oscillations are attributed to oscillations in the ^{4}He-^{4}He atom scattering amplitude of the interacting ^{4}He atoms[11] which has been shown[24] to lead to oscillations in $S(Q,\omega)$.

This paper is one of a series of investigations of $n(\mathbf{p})$ and FS effects in quantum liquids under conditions of excellent and well-understood instrumental resolution and high count-

ing statistics. The principal aim of the present paper is to examine the crossover of $S(Q,\omega)$ from the collective ($0<Q<3.5$ Å^{-1}) to the incoherent region ($Q>12$ Å^{-1}) in normal liquid ^{4}He with a less complete study of the superfluid. A detailed description of the experimental method and data reduction procedure will be given. We will employ a method of data analysis that enables FS effects and $n(\mathbf{p})$ in the normal phase to be separated. Preliminary reports of this work are to be found in Refs. 25 and 26 and complementary studies, i.e., at higher Q, in the superfluid phase and using different analysis methods are to be found in Refs. 27 and 28. A full analysis of data taken for superfluid ^{4}He will be dealt with in a later paper[28] of this series.

In this paper we cover the momentum transfer region from about 3 to 17 Å^{-1}. Deviations from the IA are important in this range and we use the method developed by Glyde[8,29] to separate the contributions to $S(Q,\omega)$ that depend on $n(\mathbf{p})$ from those that depend on FS effects. This is based on expanding the intermediate scattering function $S(Q,t)$ in powers of time. We have analyzed our data using the Glyde procedure in its simplest form, applicable only in the normal fluid phase, where the momentum distribution is nearly Gaussian. In this form, deviations of the momentum distribution from a Gaussian and FS contributions are expressed as a series of additive terms, which in the incoherent limit is similar to an expression by Sears.[4] We denote this analysis procedure as the additive approach (AA). In the superfluid phase where there is a condensate, $S(Q,t)$ has a long-time tail making an expansion in powers of t inappropriate. To capture the narrow condensate component in $S(Q,\omega)$, the convolution approach (CA) should be used. These two approaches enable the separation of FS effects from the measured $S(Q,\omega)$. For examples of the use of these two procedures in analyzing recent ^{4}He data, see Refs. 8, 26, and 27. In the present paper, only the data taken in the normal fluid phase are considered and we use the Glyde AA procedure for analysis of the data.

The paper is organized as follows. Following the Introduction, we describe the details of the experimental setup and the data reduction procedure, followed by Sec. III, in which the data are presented. Section IV describes the analysis in terms of the AA procedure, in which the various components to $S(Q,\omega)$ are separated. Their different Q dependences are used to extract the momentum distribution in the normal fluid state, which is seen to be significantly non-Gaussian. The paper ends with a discussion section.

II. EXPERIMENT

A. Experimental details

The experiment was carried out on the MARI spectrometer of ISIS, Rutherford Appleton Laboratory, U.K. MARI is a direct-geometry time-of-flight spectrometer, i.e., one in which the incident neutron beam is pulsed and monochromatic and the energy $\hbar\omega$ and momentum $\hbar Q$ transferred to the sample are obtained by recording the scattering angle and time of flight of each scattered neutron. Neutrons at ISIS are produced by nuclear spallation by directing a pulsed beam of high-energy protons onto a heavy-metal target (tungsten or uranium). The resulting fast neutrons are then thermalized in a range of moderators. The incident neutron energy on

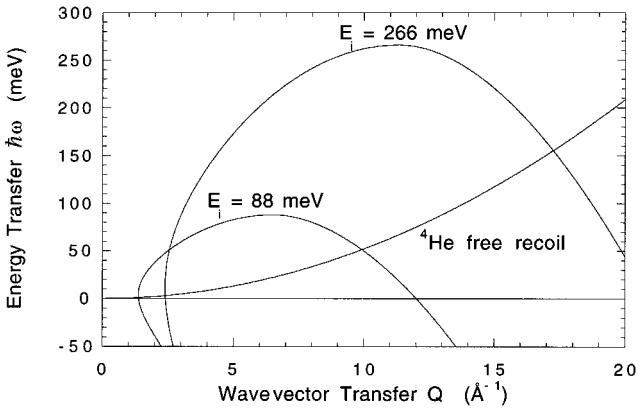

FIG. 1. Region in Q-ω covered on MARI with the two different incident energies used. Also shown is the recoil line $\hbar\omega_r = \hbar^2Q^2/2m$ for free ^{4}He atoms.

MARI is selected by the phasing of a high-speed Fermi chopper relative to the injection time of protons onto the target. MARI provides a unique combination of high flux of neutrons in the $E_i=100-1000$ meV range with good energy resolution (1–2% of E_i). Moreover, due to the large angular coverage of the detectors, a large part of the Q-ω plane can be covered in a single measurement; more than 400 ^{3}He detectors cover a continuous range of scattering angles from 3° to 135°.

A cylindrical aluminum sample cell of volume 130 cm^3, with cadmium spacers placed 1 cm apart inside in order to minimize multiple scattering, was mounted inside an ILL-type ''orange'' helium-flow cryostat and the temperature was monitored with a calibrated carbon resistor mounted on the sample cell. High-purity gaseous helium was led through a cold trap at 77 K to freeze out impurities before being condensed into the cell.

Three separate data sets were collected. The first two ($T=1.42$ and 2.50 K) used an incident neutron energy E_i of 88 meV and the third ($T=2.5$ K) was obtained using an E_i of 266 meV. The choice of these two incident energies allowed coverage of the momentum transfer ranges $2-10$ Å^{-1} and $3-17$ Å^{-1} for $E_i=88$ and 266 meV, respectively. Figure 1 shows the region in the Q-ω plane covered at the two incident neutron energies with the range of detector angles available on MARI. For the $E_i=88$ meV runs, the measured sample temperature was very stable, with fluctuations of less than 0.03 K over the time of the runs. However, due to the very long run time of the $E_i=266$ meV run, the sample temperature fluctuations were somewhat larger in this case, giving an estimated error in the sample temperature of 0.1 K.

At both incident energies, the scattering was measured with the empty cell and the cell filled with liquid helium, so that the ^{4}He scattering could be extracted by subtracting the ''empty cell'' Al scattering. The run with $E_i=266$ meV was by far the longest, extending over approximately 50 h and thus had very high counting statistics. For this measurement, a run with the empty sample cell lined on the inside with absorbing cadmium was recorded in order to correct for the attenuation of the cryostat and sample cell scattering due to the liquid ^{4}He. The effect of omitting this correction for the $E_i=266$ meV data is a small, but statistically significant oversubtraction on the low-energy side of the ^{4}He recoil

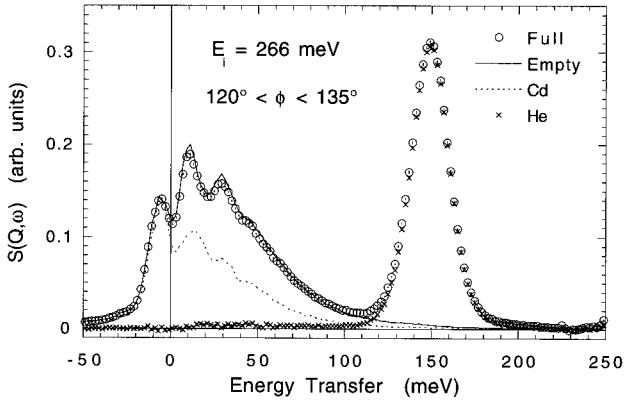

FIG. 2. Observed scattering intensity in the high-angle banks ($120° < \phi < 135°$) for $E_i = 266$ meV. Data are shown for the cell filled with ^{4}He, the empty cell, and the empty cell lined with Cd. Also shown as ''He'' is the result of performing the sample-dependent background subtraction with a transmission of 88%, described in Sec. III B. The scattering below 100 meV arises from the time-shifted Al elastic scattering from the cryostat walls and the Al phonon density of states.

peak. This is a small correction, not normally applied for weakly scattering samples (transmission $\approx 90\%$) and statistically insignificant for the $E_i = 88$ meV data.

In order to correct for the variation of detector efficiencies across the detector banks, a vanadium (incoherent scattering) run was recorded with the monochromating chopper removed, allowing neutrons of all wavelengths (''white beam'') to reach the vanadium sample, which increases the signal by several orders of magnitude.

B. Data reduction

The fast-neutron background was subtracted, as was the cryostat and empty-cell scattering. For the $E_i = 266$ meV data set, corrections were also made for the sample dependence of the cryostat and sample cell scattering, by making use of the cadmium run as follows. The transmission T of the neutron beam through the helium in the sample cell was calculated using the expression of Sears[30] to be 88.0%, and by a numerical integration over the sample cell volume to be 87.8%. This must be known to make use of the Cd background run. I is the observed scattering and subscripts f, MT, and Cd refer to the runs recorded with the cell full of helium, the empty cell, and the cell lined with Cd, respectively. The background scattering which is *independent* of the sample is I_{Cd} and the sample-*dependent* background scattering is $I_{\mathrm{MT}} - I_{\mathrm{Cd}}$. Clearly only the sample-dependent scattering is attenuated by the helium and hence the scattering from the helium in the sample cell is given by

$$I_{\mathrm{He}} = I_f - T(I_{\mathrm{MT}} - I_{\mathrm{Cd}}) - I_{\mathrm{Cd}} = I_f - TI_{\mathrm{MT}} - (1-T)I_{\mathrm{Cd}}. \quad (2)$$

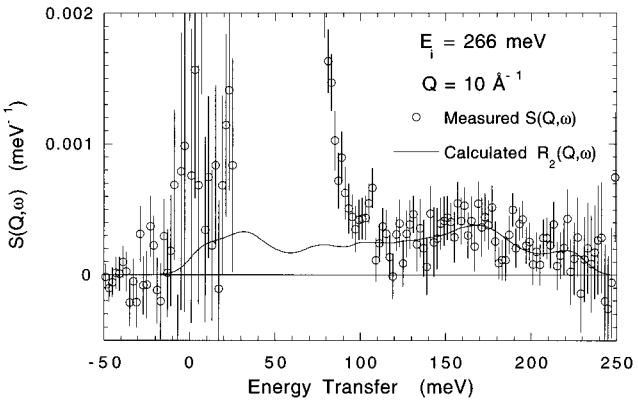

FIG. 3. Detail of the normalized scattering intensity at $Q = 10\ \text{Å}^{-1}$ measured with $E_i = 266$ meV after subtraction of the sample-dependent background, shown together with the calculated double scattering $R_2(Q,\omega)$ (Ref. 32). The remaining background is seen to be taken wholly into account.

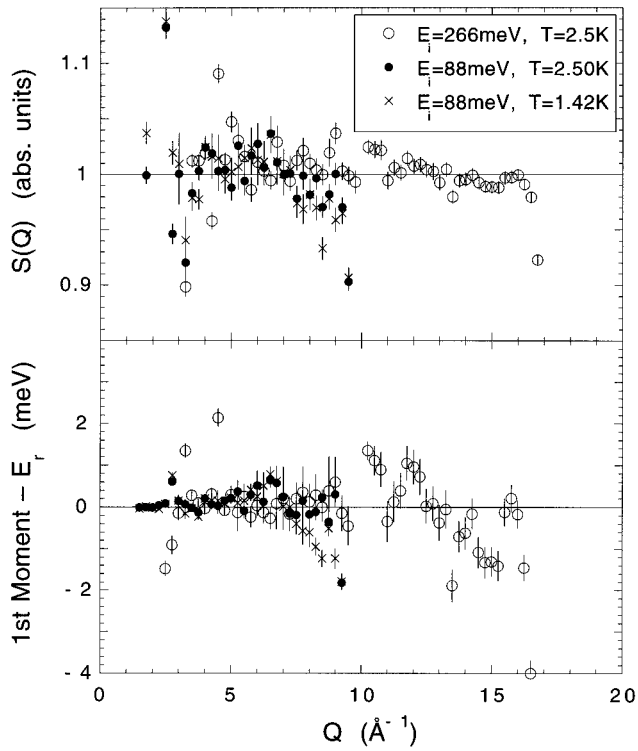

FIG. 4. Upper frame: $S(Q)$ obtained from the data by integrating all counts in the peak region at each Q. A single scale factor was used at all Q's for each data set. Lower frame: First moment of the observed scattering as a function of Q with the recoil energy subtracted.

Figure 2 shows the scattering observed in the high-angle banks ($120° < \phi < 135°$) in these three configurations and the ^{4}He scattering after subtraction of the background. The individual efficiencies of the detectors were corrected for using the ''white beam'' vanadium scattering intensities. The data were converted from their original format of neutron counts versus time-of-flight in each of the 400 detectors into $S(Q,\omega)$ along lines of constant scattering angle in the Q-ω plane and then rebinned[26,31] onto constant-Q spectra with a Q width ΔQ of $0.25\ \text{Å}^{-1}$ and an energy bin width of 1.0 meV. Using the semianalytic method of Sears,[32] the shape and magnitude of the multiple scattering was calculated by constructing model scattering functions to describe both the ^{4}He and Al sample cell and cryostat scattering. The calculated multiple scattering included both He-He and He-Al double scattering. The ratio of double to single scattering for the present sample geometry was found to be 3.3%.[30] Figure

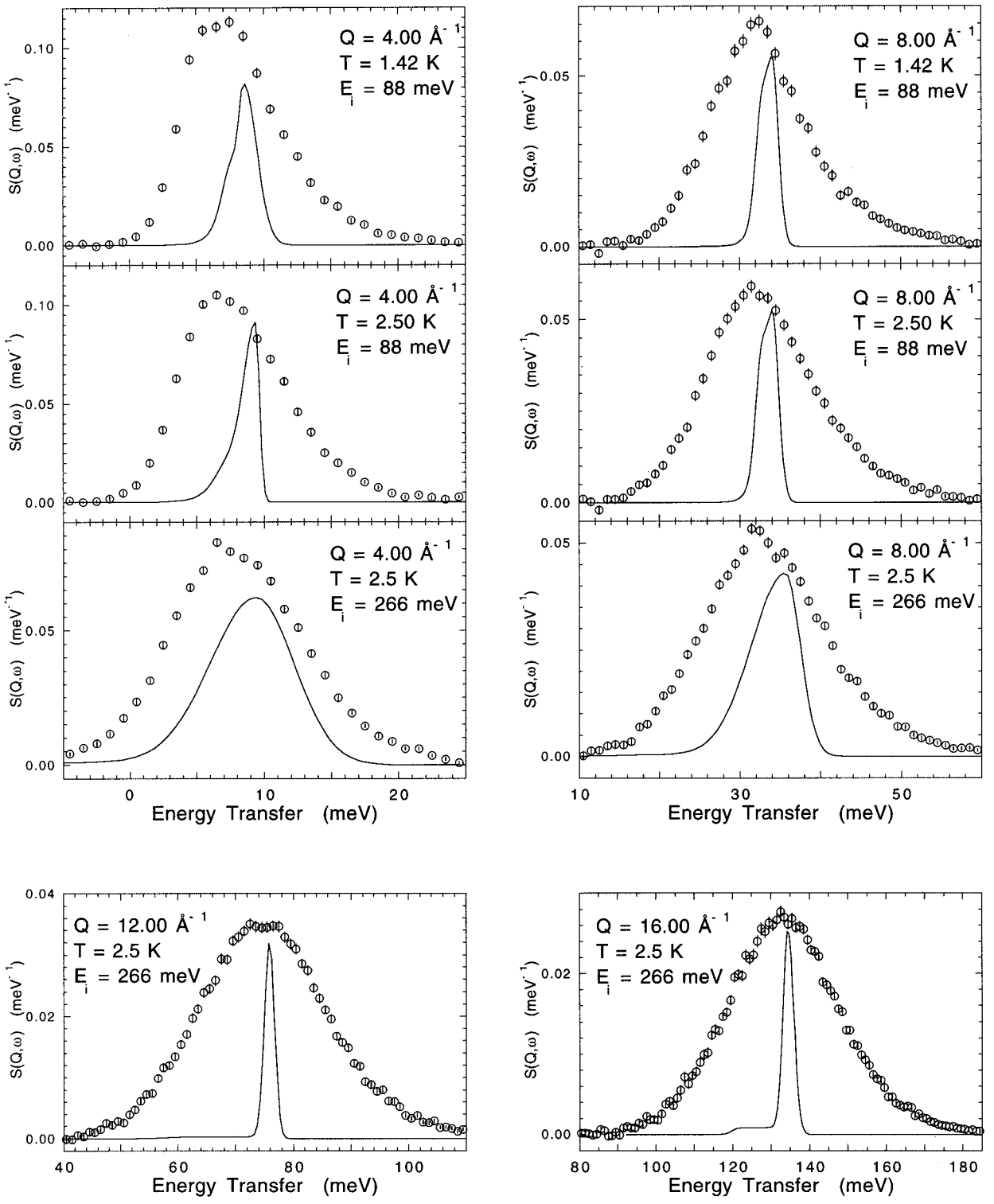

FIG. 5. Examples of the measured $S(Q,\omega)$ of liquid ^{4}He at selected wave vectors. Also shown is the calculated resolution function (solid line), obtained as described in the text, which has been shifted for clarity to lie at the recoil position $\hbar\omega_r$.

3 shows an example of the scattering remaining after subtraction of the cryostat and sample cell scattering, compared with the calculated double scattering. The remaining background is seen to be taken wholly into account by the double scattering, which was calculated and subtracted at all Q's.

The energy scale was refined using the f-sum rule, which requires that the first moment of $S(Q,\omega)$ be the recoil energy $\hbar\omega_r$ [see Eq. (1)]. In order to satisfy this requirement, a 5-mm correction to the position of the monochromatic beam monitor was required. The absolute intensity normalization was obtained from the requirement that $S(Q)=1$ in the incoherent regime ($Q>10$ Å^{-1}). A single scale factor for each data set was used for this intensity normalization. Figure 4 shows the $S(Q)$ extracted from the data, where it can be seen that the absolute intensity normalization is accurate to approximately 1% for $Q>10$ Å^{-1}. The difference be-

tween the first moment obtained from the data and the recoil energy is also shown here. It can be seen that systematic errors in both the intensity normalization and the energy scale calibration have been reduced to the level where they are comparable to the statistical errors in the counting. The $S(Q)$ and first moment shown in Fig. 4 fall off at $Q > 16$ Å^{-1} because data covering only part of the full ω range is collected (see Fig. 1).

In order to calculate the resolution function accurately, a Monte Carlo simulation program was written to describe the spectrometer.[33] The speed distribution of neutrons in the moderator was modeled by the Ikeda-Carpenter (IC) function.[34] The chopper transmission and IC function parameters were found by fits to the monitor peak shapes. The resultant simulated neutron pulse was then allowed to scatter from a model scattering function at the sample position of the same geometry as that used in the experiment. The model scattering function consisted of an IA $S(Q,\omega)$, assuming a Gaussian $n(p)$ with a realistic width. The simulated neutron pulse was scattered into each of the 400 detectors, using the actual detector geometry. The simulated time-of-flight data were then transformed into $S(Q,\omega)$ and rebinned onto constant-Q scans in the same way as was done for the real data. In this way any systematic errors introduced into the data by the data reduction procedure were reproduced in the simulated data. The effective resolution line shape was extracted at each Q by fitting the intrinsic Gaussian $S(Q,\omega)$ function to the simulated data at constant Q, convoluted with a model resolution. The model resolution function was described by a peak shape function with eight degrees of freedom, which were free parameters in the fit. This procedure gave fits with a reduced χ^2 between 1.0 and 1.2 and the resultant best-fit resolution functions were used in the subsequent data analysis. For a more detailed description of the resolution calculation, see Ref. 33.

Figure 5 shows examples of the normalized MARI data with the corresponding resolution line shapes obtained as described above. It is seen that the resolution function apparently varies with temperature, e.g., at $Q = 4.00$ Å^{-1}. This is due to instabilities in the neutron detectors on MARI. Their efficiency and intrinsic background level change with time and when the noise level becomes unacceptably high, the signal is no longer used. The number of ''bad'' detectors changed slightly between the $T = 1.42$ K and 2.50 K runs. When the data are rebinned onto constant-Q scans this causes a slight change in the effective resolution function. This effect is particularly marked for the $Q = 4.00$ Å^{-1} measurement at $E_i = 88$ meV, but is otherwise negligible.

III. COHERENCE EFFECTS AND GLORY OSCILLATIONS

As seen in Fig. 5, the measured $S(Q,\omega)$ cannot be adequately described by a single Gaussian function. The width [full width at half maximum (FWHM)] and peak position were extracted from the present data by fitting a flexible function consisting of a combination of Gaussians and exponentials spliced together and convoluted by the calculated instrumental resolution. The function used has no physical basis and was selected only on the basis that it reproduced the data well and provided a means of extracting the width and peak position. The peak position was defined as the mean of the two half-height positions.

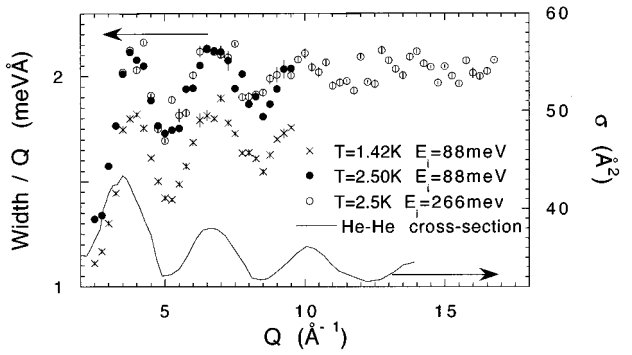

FIG. 6. Width (FWHM) of the measured $S(Q,\omega)$, obtained as described in the text, divided by Q. Also shown, on the right-hand scale, is the ^{4}He-^{4}He scattering cross section (Ref. 35). Error bars shown are the uncertainties $\pm\sigma$ in the best-fit values and may not accurately reflect the statistical uncertainties shown by the scatter of the points.

Previous measurements in the wave-vector range $4 < Q < 12$ Å^{-1} (Refs. 11 and 23) have shown oscillations in the width and peak position of the scattering function as a function of Q. These are related to oscillations in the ^{4}He-^{4}He scattering cross section, which are caused by atomic interference effects when probing the steep-core part of the atom-atom potential, and are known as ''hard-sphere glory'' oscillations.

Figures 6 and 7 show the extracted widths and peak positions as a function of Q. It is seen that the two data sets at $T = 2.5$ K are in very good agreement, indicating that the data reduction procedure and resolution calculation have reduced systematic errors to a very low level. The peak position is independent of temperature, while the width clearly increases from 1.42 to 2.5 K. Oscillations, independent of temperature, in both the width and peak position are clearly visible and are seen to continue up to at least $Q = 10$ Å^{-1}. The ^{4}He-^{4}He cross section measured by atomic beam scattering experiments[35] is also shown in the figures. It is seen that the period and phase of the oscillations is identical for the width of $S(Q,\omega)$ and the cross section, while the position oscillations are about $-\pi/2$ out of phase with the cross-section measurements. The fact that the peak position is consistently below the recoil frequency ω_r does not indicate a violation

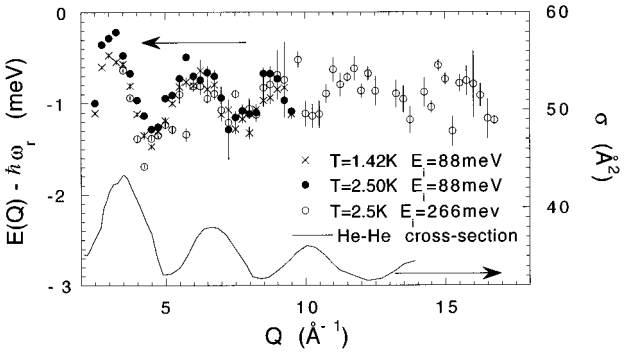

FIG. 7. Peak position of the measured $S(Q,\omega)$, obtained as described in the text, with the recoil energy $\hbar\omega_r$, subtracted. The ^{4}He-^{4}He scattering cross section (Ref. 35) is also shown on the right-hand scale. Error bars as in Fig. 6.

of the f-sum rule, but is due to the measured peak shapes having significant high-energy tails. This is clearly seen in Fig. 5. Previous neutron and x-ray-scattering measurements[19] have shown that $S(Q)$ reduces to 1 at $Q>6$ Å^{-1}, which is often taken as the lower limit for validity of the incoherent approximation. However, the oscillations observed in this study are evidence of the continuation of coherence effects, extending up to a wave vector in excess of 10 Å^{-1}, in agreement with previous studies.[11,23] Figure 7 shows that the difference between the peak center and the recoil energy does not approach zero as Q increases, but approaches a constant value of about -1 meV. This is evidence of the continuing importance of FS effects at wave vectors above the measured Q region. Since the peak width increases proportionally to Q, the shift in the peak center relative to the recoil energy will be increasingly difficult to observe as Q is increased.

IV. MOMENTUM DISTRIBUTION AND FINAL-STATE EFFECTS

From a straightforward expansion[8,21] of the coherent $S(Q,t)$ in powers of t, $S(Q,\omega)$ is obtained in terms of a Gaussian IA result $\tilde{S}_{\rm IA}(Q,\omega)$ plus corrections S_1, S_2, etc. arising from non-Gaussian components of the momentum distribution and from FS interactions:

$$S(Q,\omega)=\tilde{S}_{\rm IA}(Q,\omega)+S_1(Q,\omega)+S_2(Q,\omega)+S_3(Q,\omega)+\cdots, \tag{3}$$

where

$$\tilde{S}_{\rm IA}(Q\omega)=\frac{S(Q)}{\sqrt{2\pi\mu_2}}\exp[-(\omega-\omega_r')^2/2\mu_2], \tag{4}$$

$$S_1(Q,\omega)=-\frac{\mu_3}{2\mu_2^2}(\omega-\omega_r')\left[1-\frac{(\omega-\omega_r')^2}{3\mu_2}\right]\tilde{S}_{\rm IA}(Q,\omega), \tag{5}$$

$$S_2(Q,\omega)=\frac{\mu_4}{8\mu_2^2}\left[1-\frac{2(\omega-\omega_r')^2}{\mu_2}+\frac{(\omega-\omega_r')^4}{3\mu_2^2}\right]\tilde{S}_{\rm IA}(Q,\omega), \tag{6}$$

$$S_3(Q,\omega)=\frac{\mu_5}{8\mu_2^3}(\omega-\omega_r')\left[1-\frac{2(\omega-\omega_r')^2}{3\mu_2}+\frac{(\omega-\omega_r')^4}{15\mu_2^2}\right]\tilde{S}_{\rm IA}(Q,\omega), \tag{7}$$

where $\omega_r'=\omega_r/S(Q)$. As can be seen, the corrections S_1, S_2, etc. are alternately antisymmetric and symmetric about ω_r'. The antisymmetric terms, odd in $(\omega-\omega_r)$, and the odd coefficients μ_i $(i=3,5,...)$ in them vanish if the interaction (V) and FS effects vanish. The even coefficients μ_i $(i=4,6,...)$ depend on both the moments of $n(p)$ and FS effects. The derivation of Eq. (3) begins with an expression for $S(Q,t)$ derived by Rahman, Singwi, and Sjölander[36] and generalized to the coherent regime by Gersch and Rodriguez.[3] A cumulant expansion is used to expand $S(Q,t)$ in powers of t. Including all powers up to t^5 corresponds to keeping corrections up to $S_3(Q,\omega)$ in Eq. (1). For a more detailed description of the derivation of Eqs. (3)–(7), see Refs. 8 and 21.

In the incoherent approximation many of the above parameters reduce to simple quantities:

$$\begin{aligned} S(Q)&\to 1,\\ \omega_r'&\to\omega_r,\\ \mu_2&\to q^2\overline{\alpha_2},\\ \mu_3&\to q^2\overline{a_3},\\ \mu_4&\to q^2\overline{a_4}+q^4\overline{\alpha_4}, \end{aligned} \tag{8}$$

where $q=\hbar Q/m$ is the reduced wave vector. $\overline{\alpha}$ denotes a quantity that is a function of the momentum distribution only, while the $\overline{a}$ parameters arise from the FS interactions. They are given as follows:

$$\overline{\alpha_2}=\langle p_Q^2\rangle,$$

$$\overline{a_3}=\frac{1}{6\hbar}\langle\nabla^2V(r)\rangle,$$

$$\overline{a_4}=\frac{1}{\hbar^2}\langle F_Q^2\rangle,\quad \overline{\alpha_4}=\langle p_Q^4\rangle-3\langle p_Q^2\rangle^2, \tag{9}$$

where $\hbar p_Q$ is the atomic momentum component parallel to $\mathbf{Q}$, $V(r)$ is the interatomic potential, and $F_Q=\nabla_Q V(r)$ is the force on the struck atom along $\mathbf{Q}$.

Once the parameters μ_2, μ_3, and μ_4 are determined, we may obtain the momentum distribution directly from the fitted $S(Q,\omega)$. Essentially, we have $\overline{\alpha_2}=\langle p_Q^2\rangle$ and $\overline{\alpha_4}=\langle p_Q^4\rangle-3\langle p_Q^2\rangle^2$ which characterize $n(\mathbf{p})$, while the parameters a_3 and a_4 describe the final-state effects. In the impulse approximation, the $Q\to\infty$ limit of $S(Q,\omega)$, final-state terms of $S(Q,\omega)$ are negligible. In this limit, $S(Q,\omega)\to S_{\rm IA}(Q,\omega)$, and $S_{\rm IA}(Q,\omega)$ is the longitudinal momentum distribution $n(y)$ for the one-dimensional momentum variable $y=(\omega-\omega_r)/q$, i.e.,

$$n(y)=J_{\rm IA}(y)=\frac{1}{q}S_{\rm IA}(Q,\omega). \tag{10}$$

The IA is obtained here by setting $\overline{a_3}$ and $\overline{a_4}$ equal to zero in Eq. (3), giving

$$n(y)=\frac{1}{(2\pi\overline{\alpha_2})^{1/2}}\exp(-y^2/2\overline{\alpha_2})\left\{1+\frac{\delta}{8}\left[1-\frac{2y^2}{\overline{\alpha_2}}+\frac{y^4}{3\overline{\alpha_2^2}}\right]\right\},$$

where $\delta=\overline{\alpha_4}/\overline{\alpha_2^2}$ is the excess (kurtosis) of the distribution. Thus we may obtain $n(y)$ directly from Eq. (3). The corresponding isotropic three-dimensional momentum distribution $n(\mathbf{p})=n(p_x,p_y,y)$, which is related to $n(y)$ by $n(y)=\int dp_x dp_y n(p_x,p_y,y)$, is

$$n(\mathbf{p})=\frac{1}{(2\pi\overline{\alpha_2})^{3/2}}\exp(-p^2/2\overline{\alpha_2})\times\left\{1+\frac{\delta}{8}\left[5-\frac{10p^2}{3\overline{\alpha_2}}+\frac{p^4}{3\overline{\alpha_2^2}}\right]\right\}. \tag{11}$$

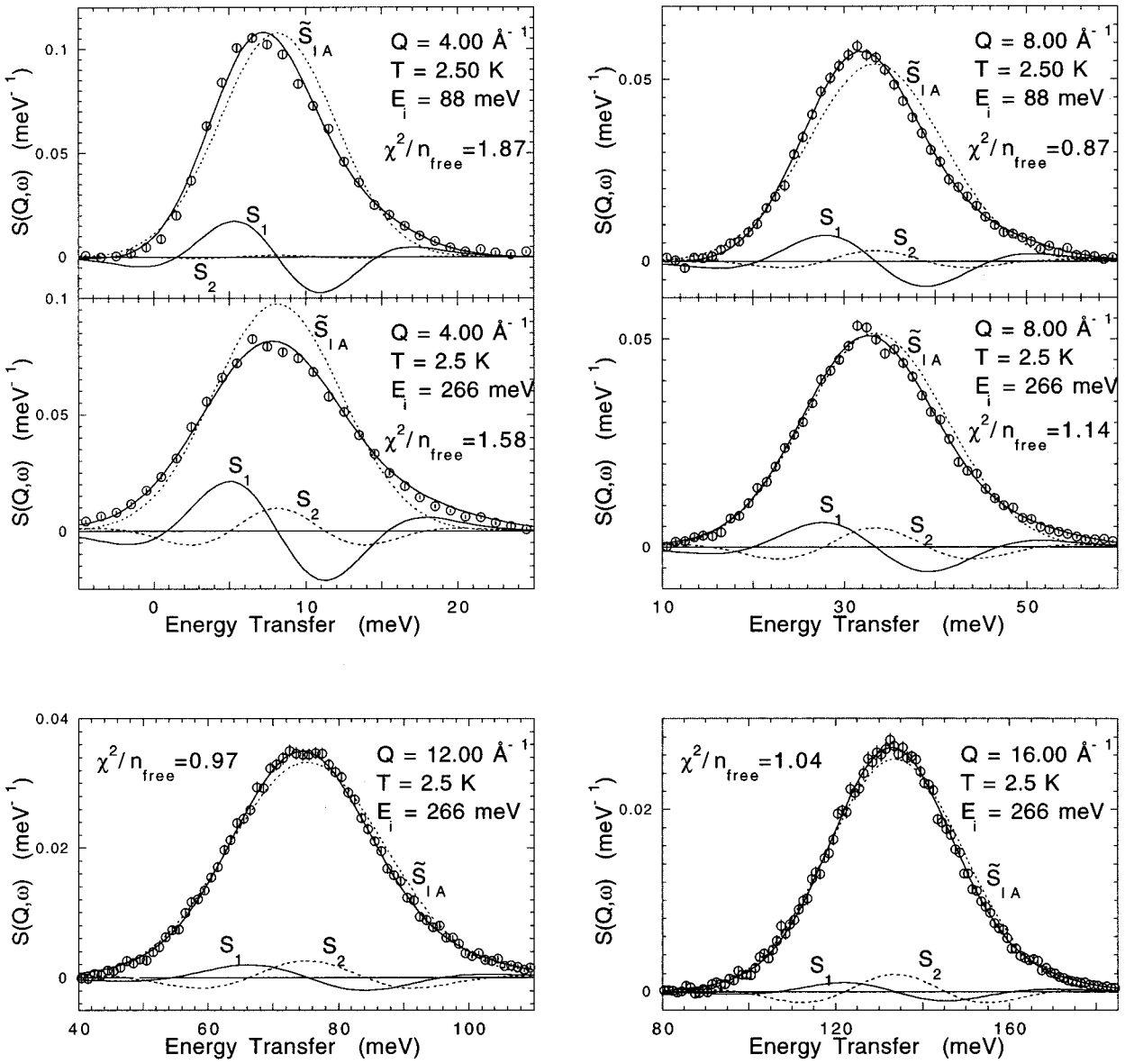

FIG. 8. Fits of the Glyde AA line shape, convoluted by the calculated resolution function. The individual components are shown separately.

Equation (11) describes a Gaussian $n(\mathbf{p})$ plus a non-Gaussian correction term. This expression is thus adequate for nearly-Gaussian momentum distributions, but cannot describe an $n(p)$ containing a low p singularity. The observed $n(\mathbf{p})$ in normal ^{4}He is obtained by fitting $S(Q,\omega)$ to data at several Q values in the incoherent limit to determine accurate values of $\overline{\alpha_2}$ and $\overline{\alpha_4}$. We shall see that this expression, using parameter values taken from the present data, can describe the momentum distribution in the normal fluid state well.

The Glyde AA expression for $S(Q,\omega)$ [Eq. (3)], convoluted by the calculated resolution function, was fitted to the data at each Q with the μ_i as free parameters. It was found that the quality of fit was unaffected by whether or not the S_3 term was included. Since S_1 and S_3 are similar, antisymmetric terms, they would compensate for each other when allowed to vary freely in the fits. In the following analysis, μ_5 was set to zero, corresponding to omitting the S_3 term from Eq. (3). The values of $S(Q)$ used in Eq. (4) were taken from Ref. 37 and were not fitted. There were thus only three free parameters in the fits: μ_2, μ_3, and μ_4. The best-fit line shapes were in good agreement with the data, the fits generally giving reduced χ^2s between 1.1 and 1.4. Examples of the fits obtained are shown in Fig. 8. It is seen that Eq. (3) is able to reproduce the observed line shape very well with only three free parameters. It is worth noting how the S_1 component decreases in amplitude with Q, while S_2 remains important at all wave vectors, which reflects their different physical origin. S_1 is a FS effect, which becomes less important as Q increases, while S_2 arises mainly from the non-Gaussian shape of the momentum distribution, as will be shown below, and is thus still present in the IA (i.e., at infinite Q).

Comparison of the parameter values obtained from the E_i=88 and 266 meV measurements provides a test of the systematic errors and the accuracy of the calculated resolution line shape. Figure 9 shows the best-fit μ_2, μ_3, and μ_4

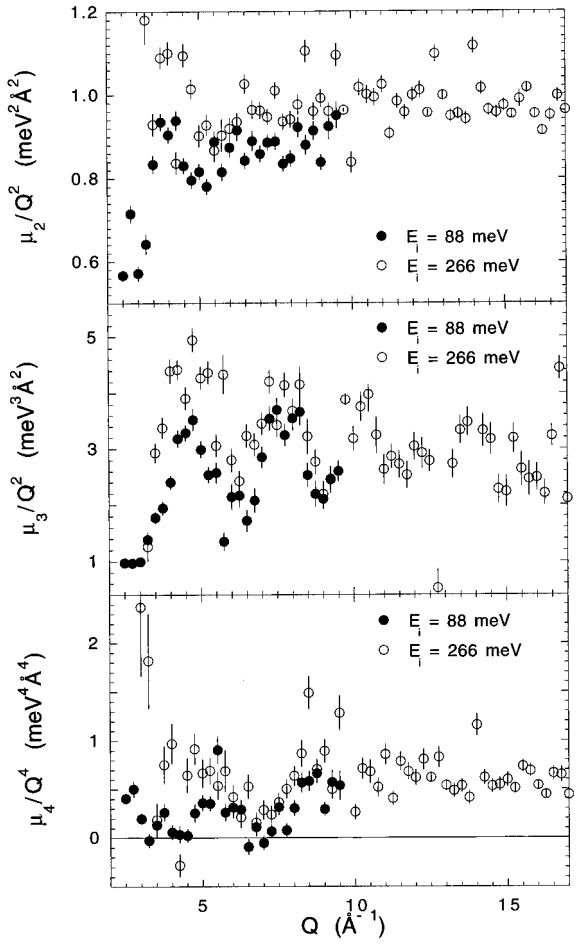

FIG. 9. Results of the AA fitting. Values of the best-fit μ_i as a function of Q, divided by Q^2 or Q^4 as stated in the axis labels. Error bars as in Fig. 6.

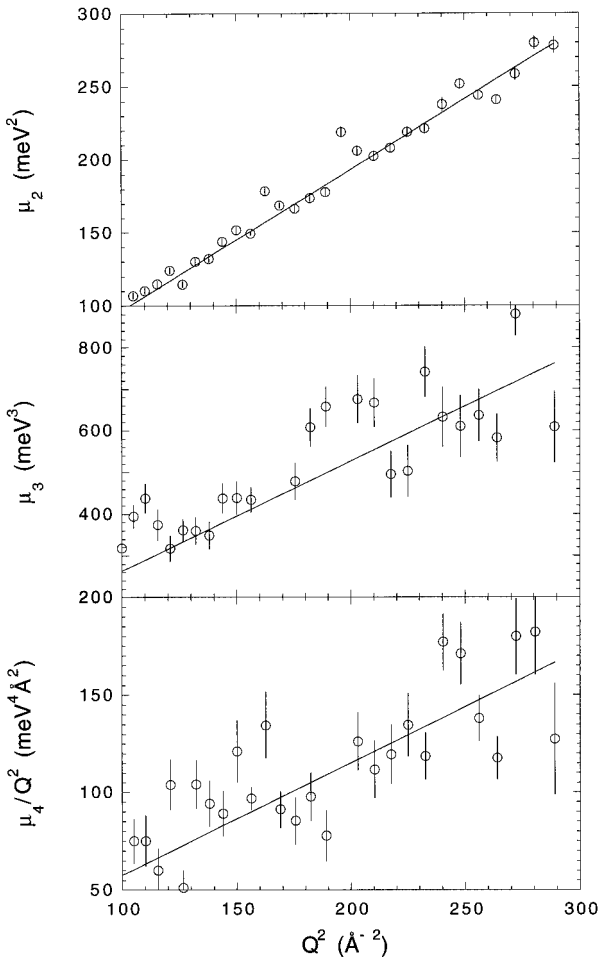

FIG. 10. The best-fit values of μ_2, μ_3, and μ_4/Q^2 as a function of Q^2 for the Q's measured in the incoherent regime. The solid line is the result of fitting Eq. (8) to the data. The data are seen to scale with Q as expected. Error bars as in Fig. 6.

parameters from the two data sets. They are seen to be in good agreement, indicating that the data are free from important systematic errors.

At large Q, μ_2/Q^2, μ_3/Q^2, and μ_4/Q^4 are seen to approach constant values, indicating that the μ parameters are scaling as expected in the incoherent regime and can be described by Eq. (8). Figure 10 shows the results of fitting Eq. (8) to the extracted μ_i parameters at $Q>10$ Å^{-1}, in the incoherent regime. In this way we obtain estimates for $\overline{\alpha_2}$, $\overline{\alpha_4}$, and $\overline{a_3}$. The $\overline{a_4}$ parameter was found to be zero within the precision of the determination and was set to zero during the fitting. The best-fit values are given in Table I. From Eq. (9) we can use $\overline{\alpha_2}$ to calculate an estimate for $\langle K\rangle$, the mean kinetic energy per atom, a quantity of fundamental interest in liquid ^{4}He. We obtain

$$\langle K\rangle=\frac{3}{2}\frac{\hbar^2}{m}\langle p_Q^2\rangle=14.8\pm1.0\ \text{K}\ \ (E_i=88\ \text{meV data})$$

$$=16.1\pm0.5\ \text{K}\ \ (E_i=266\ \text{meV data}).$$

These values are in good agreement with the value of 15.9 K inferred by Sears[38] from a compilation of of neutron scattering measurements, with the values obtained by Sosnick, Snow, and Sokol[16] from neutron scattering data at $Q=23$ Å^{-1} (16.1 K at $T=2.3$ K), with that of Azuah *et al.*[27] (16.3±0.35 K at $T=2.3$ K obtained using the CA applied to higher-Q neutron data) and with the value of 16.0 K obtained by path integral Monte Carlo calculations (PIMC) (Ref. 39).

Figures 9 and 10 show that μ_4 scales as Q^4 in the incoherent regime. The coefficient α_4 is obtained by fitting $\mu_4=\overline{\alpha_4}(\hbar Q/m)^4$ to the data as in Fig. 10, from which the excess of $n(\mathbf{p})$ is found as $\delta=\overline{\alpha_4}/\overline{\alpha_2^2}$ (given in Table I). With the best-fit values for $\overline{\alpha_2}$ and $\overline{\alpha_4}$ the momentum distribution is given by Eq. (11). This is plotted in Fig. 11 along with the $n(\mathbf{p})$ obtained from a PIMC by Ceperley and Pollock,[39] which is seen to be in good agreement. The error bar shows the uncertainty in the extracted $n(\mathbf{p})$, which arises from the error in the value of the excess, δ, extracted from the data.

TABLE I. Best-fit parameters of Eq. (9) from the fits shown in Fig. 10. $\overline{a_4}$ was negligible.

μ_2/Q^2 (meV^2 Å^2)	μ_3/Q^2 (meV^3 Å^2)	μ_4/Q^4 (meV^4 Å^4)
0.965±0.03	2.6±0.5	0.58±0.12

$\overline{\alpha_2}$ (Å^{-2})	$\overline{\alpha_4}$ (Å^{-4})	δ	$\overline{a_3}$ (meV Å^{-2})
0.886±0.030	0.49±0.10	0.62	2.38±0.50

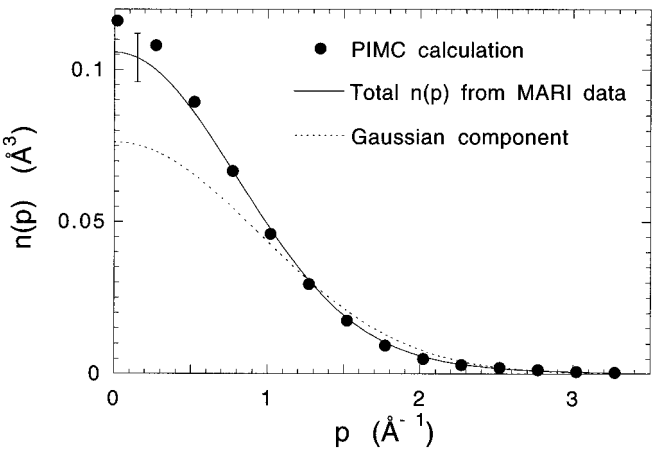

FIG. 11. The momentum distribution at $T=2.5$ K calculated using Eq. (11) with the second and fourth moments obtained from the best-fit μ_2 and μ_4 parameters in the incoherent regime. The results of a PIMC calculation of Ceperley and Pollock (Ref. 39) also at $T=2.5$ K are seen to be in good agreement. Also shown is the Gaussian component of the momentum distribution extracted from our data.

Also shown is the Gaussian component of the $n(\mathbf{p})$ extracted from our data, which is constructed by setting $\delta=0$. Since the first (Gaussian) term contains the entire second moment of $n(\mathbf{p})$, the Gaussian component shown is also consistent with the value of $\langle K\rangle$ obtained from our data. It is clear that the momentum distribution in the normal fluid is significantly different from a Gaussian.

Figure 11 can be compared with Fig. 2(a) of Ref. 27, which shows $n(\mathbf{p})$ extracted using the CA from higher-Q neutron scattering data at $T=2.3$ K. The extracted momentum distributions are very similar, except at small p (below $p\approx 0.4$ Å^{-1}) where Ref. 27 shows a slightly more peaked distribution. A small term proportional to $\langle p_Q^6\rangle$ beyond the analysis here was found in Ref. 27 that increases the intensity at the center of the peak. A more peaked distribution is also consistent with the lower measuring temperature of 2.3 K.

V. DISCUSSION AND CONCLUSION

Previous measurements of $S(Q,\omega)$ of liquid ^{4}He at intermediate to high wave vector have either concentrated on selected Q values or, in the case of time-of-flight measurements, have collected data over only a narrow range of scattering angles, in which case Q varies as a function of ω.

MARI contains a very large number of detectors, covering a wide and continuous range of scattering angles. This has enabled us to rebin our data to constant Q from the lines of constant scattering angle in the Q-ω plane, at which they are necessarily measured in a time-of-flight neutron-scattering experiment. As a result, we are able to analyze our data in terms of $S(Q,\omega)$ at constant Q and extract parameters valid at that particular wave vector. The rebinning to constant Q can then be performed systematically, such that the data can be transformed into a number of constant-Q scans covering the measured Q-ω region. We can thus extract parameters describing the measured $S(Q,\omega)$ at each wave vector and observe their Q dependence. In this way we can observe the approach towards the incoherent approximation and the IA. By fitting to the Glyde AA expression, we can extract parameters whose Q dependence is sensitive to the shape of the momentum distribution.

This method of data analysis was made possible by the high quality of the data and the wide range in Q-ω space covered by the experiment. The data are of such high statistical precision that we are vulnerable to even very small systematic errors arising from inconsistencies in the data reduction procedure. For this reason, some effort has gone into the data reduction procedure as well as the calculation of the instrumental resolution.

We find evidence of coherence effects continuing up to a wave vector in excess of 12 Å^{-1}, observed through oscillations in both the width and position of $S(Q,\omega)$. In the incoherent limit ($Q>12$ Å^{-1}) the parameters μ_2/Q^2, μ_3/Q^2, and μ_4/Q^4 appearing in $S(Q,\omega)$ become independent of Q. The data at constant Q are fitted to the Glyde AA expressions and a good fit is obtained with only three free parameters. The mean kinetic energy per atom $\langle K\rangle$ is extracted and found to be consistent with earlier determinations. A functional form for the momentum distribution $n(\mathbf{p})$ in the normal fluid phase is obtained in Eq. (11). Using parameters determined in the AA fits, we find the momentum distribution of liquid ^{4}He at $T=2.5$ K shown in Fig. 11, and obtain very good agreement with a PIMC by Ceperley and Pollock.[39] Interestingly, the extracted $n(\mathbf{p})$ is clearly non-Gaussian in a way that is consistent with a preferential occupation of low-momentum states above the condensation temperature. This is completely different from the case of liquid Ne, in which $n(\mathbf{p})$ is well described by a Gaussian and the only observable quantum effect is the broadening of $n(\mathbf{p})$ arising from the zero-point motion.[27]

Elsewhere,[28] data for both the normal and superfluid phases, covering a wider Q range, are presented and analyzed using the convolution approach. In the CA, both the momentum distribution and the final-state function are recovered as full single functions and not as additive components. This enables the use of more complicated momentum distribution models including those with a singular behavior, as is expected for superfluid ^{4}He where there is a δ-function peak representing the condensate fraction. The paper will focus on the evaluation and extraction of the momentum distribution. On the basis of the Q dependence of the fitted parameters, a ''scaled'' final state function will be extracted and its properties and significance discussed.

ACKNOWLEDGMENTS

The authors are grateful to the staff of the ISIS facility of the Rutherford Appleton Laboratory. The technical assistance of Z. A. Bowden and I. Bailey is gratefully acknowledged, as are the help and stimulating discussions with A. D. Taylor, S. M. Bennington, and R. T. Azuah. We are grateful to the Engineering and Physical Sciences Research Council for financial support. K.H.A. would like to thank the I.L.L. and the Japan Society for the Promotion of Science (J.S.P.S.) for financial support during this work. H.R.G. gratefully acknowledges the National Science Foundation through Grant Nos. INT-9314661 and DMR-9623961.

*Present address: Department of Physics, University of Liverpool, Oxford Street, Liverpool L69 3BX, U.K.

[1] S. W. Lovesey, *Theory of Neutron Scattering from Condensed Matter* (Oxford University Press, Oxford, 1984), Vol. 1.
[2] *Momentum Distributions*, edited by R. N. Silver and P. E. Sokol (Plenum, New York, 1989).
[3] H. A. Gersch and L. J. Rodriguez, Phys. Rev. A **8**, 905 (1973).
[4] V. F. Sears, Phys. Rev. B **30**, 44 (1984), and references therein.
[5] R. N. Silver, Phys. Rev. B **37**, 3794 (1988); **38**, 2283 (1988); **39**, 4022 (1989).
[6] A. S. Rinat, Phys. Rev. B **42**, 9944 (1990), and references therein.
[7] C. Carraro and S. E. Koonin, Phys. Rev. Lett. **65**, 2792 (1990).
[8] H. R. Glyde, Phys. Rev. B **50**, 6726 (1994).
[9] A. Miller, D. Pines, and P. Nozières, Phys. Rev. **127**, 1452 (1962).
[10] P. C. Hohenberg and P. M. Platzmann, Phys. Rev. **152**, 198 (1966).
[11] P. Martel, E. C. Svensson, A. D. B. Woods, V. F. Sears, and R. A. Cowley, J. Low Temp. Phys. **23**, 285 (1976).
[12] V. F. Sears, E. C. Svensson, P. Martel, and A. D. B. Woods, Phys. Rev. Lett. **49**, 279 (1982).
[13] E. C. Svensson and V. F. Sears, in *Frontiers of Neutron Scattering*, edited by R. J. Birgeneau, D. E. Moneton, and A. Zilinger (North-Holland, Amsterdam, 1986).
[14] Using the Sears *et al.* method and earlier data, H. A. Mook, Phys. Rev. Lett. **51**, 1454 (1983).
[15] T. R. Sosnick, W. M. Snow, P. E. Sokol, and R. N. Silver, Europhys. Lett. **9**, 707 (1989).
[16] T. R. Sosnick, W. M. Snow, and P. E. Sokol, Phys. Rev. B **41**, 11 185 (1990).
[17] T. R. Sosnick, W. M. Snow, R. N. Silver, and P. E. Sokol, Phys. Rev. B **43**, 216 (1991).
[18] W. M. Snow and P. E. Sokol, in *Excitations in Two-Dimensional and Three-Dimensional Quantum Fluids*, Vol. 257 of *NATO Advanced Study Institute: Series B, Physics*, edited by A. F. G. Wyatt and H. J. Lauter (Plenum, New York, 1987).
[19] H. R. Glyde and E. C. Svensson, in *Methods of Experimental Physics, Vol. 23*, edited by D. L. Price and K. Sköld (Academic, New York, 1987), P. B, p. 303.
[20] P. E. Sokol, in *Bose-Einstein Condensation*, edited by A. Griffin, D. W. Snoke, and S. Stringari (Cambridge University Press, Cambridge, 1995).
[21] H. R. Glyde, *Excitations in Liquid and Solid Helium* (Oxford University Press, Oxford, 1994).
[22] R. A. Cowley and A. D. B. Woods, Can. J. Phys. **49**, 177 (1971).
[23] W. G. Stirling, E. F. Talbot, B. Tanatar, and H. R. Glyde, J. Low Temp. Phys. **73**, 33 (1988).
[24] B. Tanatar, E. F. Talbot, and H. R. Glyde, Phys. Rev. B **36**, 8376 (1987).
[25] K. H. Andersen, W. G. Stirling, H. R. Glyde, R. T. Azuah, S. M. Bennington, A. D. Taylor, Z. A. Bowden, and I. Bailey, Physica B **197**, 198 (1994).
[26] K. H. Andersen, Ph.D. thesis, Keele University and Institut Laue-Langevin, 1991.
[27] R. T. Azuah, W. G. Stirling, H. R. Glyde, P. E. Sokol, and S. M. Bennington, Phys. Rev. B **51**, 605 (1995).
[28] R. T. Azuah *et al.* (unpublished).
[29] H. R. Glyde, Physica B **194-196**, 505 (1994).
[30] V. F. Sears, Adv. Phys. **24**, 1 (1975).
[31] K. H. Andersen, W. G. Stirling, R. Scherm, A. Stunault, B. Fåk, H. Godfrin, and A. J. Dianoux, J. Phys.: Condens. Matter **6**, 821 (1994).
[32] V. F. Sears, Nucl. Instrum. Methods **123**, 521 (1975).
[33] K. H. Andersen, Nucl. Instrum. Methods Phys. Res. A **371**, 472 (1996).
[34] S. Ikeda and J. M. Carpenter, Nucl. Instrum. Methods Phys. Res. A **239**, 536 (1985).
[35] R. Feltgen, H. Pauly, F. Torello, and H. Vehmeyer, Phys. Rev. Lett. **30**, 820 (1973); R. Feltgen, H. Kirst, K. A. Köhler, H. Pauly, and F. Torello, J. Chem. Phys. **76**, 2360 (1982).
[36] A. Rahman, K. S. Singwi, and A. Sjölander, Phys. Rev. **126**, 986 (1962).
[37] E. C. Svensson, V. F. Sears, A. D. B. Woods, and P. Martel, Phys. Rev. B **21**, 3638 (1980).
[38] V. F. Sears, Phys. Rev. B **28**, 5109 (1983).
[39] D. M. Ceperley and E. L. Pollock, Can. J. Phys. **65**, 1416 (1987).